A Computational Framework for Mechanical Response of Macromolecules: Application to the Salt Concentration Dependence of DNA Bendability

Liang Ma,[†] Arun Yethiraj,[‡] Xi Chen,[§*] and Qiang Cui[†‡*]

[†]Graduate Program in Biophysics, [‡]Department of Chemistry and Theoretical Chemistry Institute, University of Wisconsin-Madison, Madison, Wisconsin; and [§]Nanomechanics Research Center, School of Engineering and Applied Sciences, MC 4709, Columbia University, New York, New York

ABSTRACT A computational framework is presented for studying the mechanical response of macromolecules. The method combines a continuum mechanics (CM) model for the mechanical properties of the macromolecule with a continuum electrostatic (CE) treatment of solvation. The molecules are represented by their shape and key physicochemical characteristics such as the distribution of materials properties and charge. As a test case, we apply the model to the effect of added salt on the bending of DNA. With a simple representation of DNA, the CM/CE framework using a Debye-Hückel model leads to results that are in good agreement with both analytical theories and recent experiments, including a modified Odijk-Skolnick-Fixman theory that takes the finite length of DNA into consideration. Calculations using a more sophisticated CE model (Poisson-Boltzmann), however, suffer from convergence problems, highlighting the importance of balancing numerical accuracy in the CM and CE models when dealing with very large systems, particularly those with a high degree of symmetry.

INTRODUCTION

Large-scale conformational transitions are an integral part of the functional cycle of many biomolecules, especially those involved in mechano-biological processes (1). Well-known examples in this context include the conformational switchings in motor proteins under mechanical strain (2,3), the mechanical modulation of DNA conformation (bending, wrapping, supercoiling, etc.) (4–7), and the gating of mechanosensitive channels by the mechanical deformation of the lipid membrane and/or cytoskeleton (8,9). These mechano-biological processes (10) are difficult to study using simulations at the atomistic level because of the long length- and timescales involved. Consequently, there has been considerable effort devoted to coarse-graining atomistic models, in the simplest case by grouping several atoms into a united-atom. The resulting calculations can be orders-of-magnitude more efficient, but often still not sufficient to sample the desired length- and timescales.

An alternative avenue is to employ continuum mechanics (CM) models, which are particularly useful when dealing with large length scales and complex modes of mechanical perturbations. We have recently presented a hierarchical computational framework referred to as molecular-dynamics decorated finite element method (FEM) (11,12), in which key parameters in the CM model, such as properties of materials and interactions among continuum components, are extracted from relevant atomistic simulations. In this way, the CM model can potentially handle large length- and timescales while incorporating molecular characteristics specific to the system of interest. In our recent proof-of-concept studies (11,13), the molecular-dynamics decorated FEM framework has been applied to study the gating transition of bacterial mechanosensitive channel of large conductance (MscL) (8,9). Despite a host of enormous simplifications, e.g., treating the transmembrane helices as homogeneous rods, a number of features regarding the structural change of the channel during the gating transition were found in qualitative agreement with available experimental and atomistic simulation studies (14). There were some quantitative differences when compared to experiment, and one of the reasons is the neglect of solvation effects in the calculations.

The first goal of this work is to establish a computational framework to incorporate solvation effects in CM-based simulations. We combine continuum electrostatics (CE) methods (15,16), which have been widely used to model solvation of biomolecules (17,18), with CM models, leading to a combined CM/CE framework. The second goal of this work is to explore the reliability and numerical convergence of the CM/CE framework using a simple but realistic biological problem that involves large length scales and is sensitive to solvation. In particular, we chose to study the dependence of DNA bendability on salt concentration.

The mechanical deformation of DNA is important in many biological processes, such as genome packaging, DNA replication, and transcription (e.g., DNA looping (6,19)). The response of DNA molecules to mechanical forces has been probed by various experimental techniques (20,21), most recently via single molecule manipulations that stretch, bend, or twist DNA molecules (22–24). The most basic mechanical property of DNA as a polyelectrolyte is its persistence length P, which has been found to increase rather significantly as the salt concentration decreases; this is

Submitted October 15, 2008, and accepted for publication January 23, 2009.

*Correspondence: xichen@civil.columbia.edu or cui@chem.wisc.edu

Editor: Nathan Andrew Baker.

0006-3495/09/05/3543/12 $2.00

doi: 10.1016/j.bpj.2009.01.047

expected from the increased electrostatic repulsion between backbone phosphate groups as the salt concentration is lowered (22,25). The sensitivity of P to solvation and the relatively simple shape of DNA molecules (when its length is shorter or similar to P) suggest that explicitly examining the salt concentration dependence of DNA persistence length is an ideal problem for testing the combined CM/CE framework. We note that the persistence length of DNA is known to be ~500 Å at physiological condition; thus, an explicit modeling of DNA bendability ideally requires models of such length scales, for which a CM description is uniquely appropriate. Indeed, several finite element simulations on DNA deformation have been reported (26–29), although the salt dependence has only been rarely modeled explicitly (30).

The classical analytical theory that attempted to capture the salt effect quantitatively is the Odijk-Skolnick-Fixman (OSF) theory (31,32). In this theory, the DNA is described as a polyion chain of infinite length and the electrostatic and nonelectrostatic contributions to its persistence length are assumed to be as separate and additive. With a Debye-Hückel (DH) treatment of interactions between charged sites, the OSF theory calculates the difference in electrostatic energy between the straight and bent conformations of DNA in uniform bending, from which the electrostatic contribution to persistence length is extracted. Specifically, without considering sequence dependence, the persistence length P is given as (31,32)

$$P = P_{\mathrm{o}} + P_{\mathrm{el}} = P_{\mathrm{o}} + 0.324I^{-1} = P_{\mathrm{o}} + 0.324c^{-1}\text{Å}, \quad (1)$$

where P_{o} and P_{el} are the nonelectrostatic and electrostatic contributions to P, respectively; and I and c are the ionic strength and salt concentration in molar units, respectively. In this study, we are interested in the dependence of P on monovalent (e.g., NaCl) salt concentration and therefore $I = c$. Recent single molecular experiments (22,24) using λ-DNA (~10^4 bp with a contour length of 16.6 μm) found that the prediction of the OSF theory is satisfactory (e.g., within a few nanometers in (24)) for a broad range of salt concentrations, although controversies remain regarding the proper interpretation of various experimental data and basic assumptions made in the OSF theory (see (33)).

In this article, we first describe a fairly general combined CM/CE framework that allows us to explicitly model DNA deformation and therefore extract P for DNA of finite lengths at different salt concentrations. We then test several ways of treating the DNA shape and solvation effects. We show that the prediction of the CM/CE approach is in good agreement with the OSF theory, especially when the end-effect is taken into consideration (34), which serves as an important validation to the computational protocol. Rather simple models are used for DNA in this work, as the main goal is to explore the numerical behavior of the CM/CE approach instead of resolving controversies regarding DNA bendability (33) (also see Results and Discussion).

COMPUTATIONAL METHODS

The computational framework includes essentially two components: CM simulations based on FEMs, which solve for the deformed structure under specific external force (loads), and CE calculations, which compute electrostatic solvation forces using structural information. It is also possible to include nonpolar contributions to solvation (17,18), but this contribution does not depend on salt concentration (at our level of modeling). The key is to exchange information self-consistently (e.g., structures and forces) between the CM and CE components, which has been accomplished as described below. The set of models and calculations developed in this work are summarized in Table 1.

Continuum mechanics models for DNA

The first step in any CM simulations is to build the FEM model for the system under study. Two types of FEM models are built for DNA for this purpose. In the OSF theory, DNA is treated as a cylindrical polyion with equally spaced charged sites that correspond to the phosphate groups. Accordingly, simple cylindrical FEM models (referred to as the polyion models in this article) are built to make it possible to carry out a direct comparison with the OSF prediction. In addition, to explore the effect of incorporating the molecular shape information, which is straightforward to do with FEM and expected to be important for biomolecules in general, FEM models that represent the irregular molecular surfaces (referred to as the molecular-surface models in this article) and the underlying chemical composition are also constructed. To study the length dependence of the persistent length (due to end effects (35)), two DNA systems of 36 and 300 basepairs are studied.

The polyion FEM models

In the polyion FEM models, DNA molecules are modeled as cylindrical rods with the radius of 10.0 Å; the length is ~122 Å and ~1020 Å for the 36-bp and 300-bp DNA, respectively. The cylindrical rods are meshed into three-dimensional tetrahedral elements as shown in Fig. 1, *a* and *b*, for the 36-bp DNA with a smooth cap on each end (11,13). The final model consists of 1215 nodes and 4283 finite elements for the 36-bp DNA, and 6060 nodes and 24,445 finite elements for the 300-bp DNA. There are in total 70 and 598 charged sites for the 36-bp and 300-bp DNA, respectively, along the contour axis of the cylinder; the spacing between neighboring charged sites is 1.7 Å as in the OSF theory, which is half of the average basepair spacing of 3.4 Å in B-form DNAs.

TABLE 1 Continuum mechanics models and calculation parameters used in this study of DNA bendability

DNA	FEM model	$E^{0.15}$ (10^8 Pa)*	Electrostatic model†	$\lvert\vec{F}_{\mathrm{ext}}\rvert$ (pN)‡
300 bp	Polyion	2.6	DH	0.003
300 bp	Molecular surface	29.75	DH	0.003
36 bp	Polyion	2.6	DH	0.4
36 bp	Molecular surface	28.10	DH, PB	0.4

*Effective Young's modulus at 0.15 M NaCl.
†DH stands for the Debye-Hückel model, PB stands for the Poisson-Boltzmann model (see main text).
‡Magnitude of the external force applied to the right terminus of the DNA (see Fig. 2 for an illustration) in the force-based CM/CE simulations. The values are chosen such that the equilibrium bending angle is ~5°. A range of force is tested and the extracted persistence length is not sensitive when $\lvert\vec{F}_{\mathrm{ext}}\rvert$ is varied within an order of magnitude (results not included).

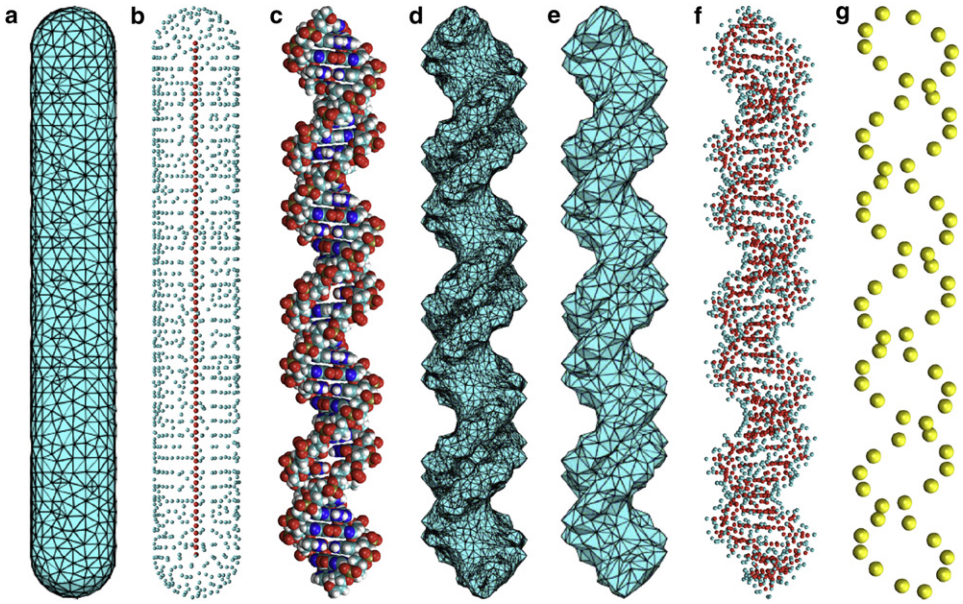

FIGURE 1 Illustration of various steps in constructing finite element method (FEM) models. (*a* and *b*) Polyion model; (*c–g*) molecular surface model for the 36-bp DNA. (*a*) Triangularized surface of the polyion model. (*b*) Nodes of the polyion model with chemical nodes (those that bear partial charges) shown in red. (*c*) Atomic structure in a van der Waals representation. (*d*) Triangularized molecular surface. (*e*) Simplified triangularized molecular surface and the volume of space enclosed by this surface discretized into tetrahedral elements. (*f*) Nodes of the molecular surface model with chemical nodes (correspond to all heavy atoms) in red. (*g*) Phosphorus nodes of the molecular surface model, which are the only nodes that bear charges in this study.

The molecular surface FEM models

To construct the molecular surface FEM models, a 12-bp DNA duplex with a sequence d(CGCGAATTCGCG)$_2$ is duplicated three (25) times to build a DNA molecule of 36 (300) basepairs. The B-form atomic structures (Fig. 1 *c* for 36-bp DNA) are obtained from the *make-na* web server and the Nucleic Acid Builder program developed by T. Macke and D. A. Case (http://structure.usc.edu/make-na/). The molecular surface (Fig. 1 *d*) of each DNA molecule is then calculated and triangularized using the MSMS program (36) with a probe water radius of 1.4 Å. The triangularized surface is then simplified by the QSLIM program (37) to reduce the number of the surface triangles to 2000 for the 36-bp DNA (Fig. 1 *e*) and 10,000 for the 300-bp DNA. The volume enclosed by this simplified surface is subsequently discretized into a three-dimensional mesh consisting of tetrahedral elements with the heavy atoms of DNA (totally 1470 and 12,294 for the 36-bp and 300-bp DNA, respectively) as input nodes. The final FEM model (Fig. 1 *e*) consists of 2655 nodes and 13,728 finite elements for the 36-bp DNA and 19,893 nodes and 106,799 finite elements for the 300-bp DNA; shown explicitly in Fig. 1 *g* are the phosphorus nodes, which are the sites that bear explicit charges in the solvation calculations (see Solvation force calculations: continuum electrostatics).

The major advantage of the molecular surface FEM models over the highly simplified cylindrical polyion models is that they take into account the molecular nature of DNA, such as its irregular shape, the major/minor grooves, and double-helical distributions of the phosphate groups. In addition, the mapping between heavy atoms of DNA and specific FEM nodes make it straightforward to define chemical nodes (*red nodes* in Fig. 1 *f*, in total 1470), which encode the key chemical characteristics of the molecule (i.e., charge distribution and solute/solvent interface) required in electrostatics solvation calculations; for simplicity, however, only the phosphorus nodes are taken to be charged in this study although the chemical nodes do contribute to the definition of the dielectric boundary in the Poisson-Boltzmann (PB) calculations (see below).

DNA materials properties

Throughout this study, the DNA is treated as homogeneous isotropic elastic material, thus only the effective Young's modulus, E, and the Poisson ratio, σ, are required to describe its mechanical properties. The Poisson ratio, σ, is taken as 0.3 for all FEM models. For the Young's modulus, the numerical value depends on the representation of the DNA and can be estimated in the following fashion. For the polyion model, as discussed in the literature (27,28,38), the Young's modulus can be extracted from the persistence length according to the relation

$$E = Pk_BT/J, \tag{2}$$

where P is the persistence length, k_B the Boltzmann constant, and T the temperature (298 K). The value J is the moment of inertia of cross section, which for a cylinder is equal to $\pi r^4/4$, where $r = 10$ Å is the radius of the cross section. Since the persistence length is ~500 Å for DNA at 0.15 M salt concentration (20,21), the effective Young's modulus (denoted as $E^{0.15}_{poly}$) can be estimated to be 2.6×10^8 N/m^2(Pa) according to Eq. 2; this is used as the reference value for simulations using the polyion model at different salt concentrations (see Salt concentration effects on DNA bendability: combining continuum mechanics and continuum electrostatics).

Since the molecular surface FEM models take into account the irregular shape of DNA molecules, different moment of inertia and Young's modulus (denoted as E^c_{mol}) need to be adapted to maintain $E \times J$ or P to be consistent with the polyion models for a fair comparison of models. Since the moment of inertia for an irregular shape is not straightforward to compute, we chose to determine the value of E^c_{mol} by matching the degree of bending in molecular surface and polyion FEM models of the same length under the same external force; in other words, the bending rigidity, and therefore the persistence length, is taken to be the same for the polyion and molecular surface FEM models. This procedure gives the reference values at 0.15 M NaCl as $E^{0.15}_{mol} = 28.10$ and 29.75×10^8 N/m^2 for the 36-bp and 300-bp DNA, respectively (summarized in Table 1).

We note that a reference persistence length of 500 Å is used for both the 36-bp and 300-bp DNAs at 0.15 M. At this salt concentration, the DH screening length is 8 Å, much smaller than the contour length of both DNAs; thus, the end effect is expected to be negligible. At lower salt concentrations, however, this is no longer true, as reflected in the different salt concentration dependence of the persistence length for the two DNA systems (see Results and Discussion).

Solvation force calculations: continuum electrostatics

To compute the solvation free energy and force at a given salt concentration, a number of implicit solvation models (17,18) can be used. In general, the solvation free energy includes both electrostatic and nonpolar contributions. With the popular surface-area model for the nonpolar contribution (17,18),

however, only the electrostatic component contributes to the differential solvation force at different salt concentrations. The key quantity for the evaluation of electrostatic solvation free energy (and force) is the charge distribution of the solute. Although the mapping procedure described above can be used to encode the charge distributions to all chemical nodes (see Fig. 1 *f*), for this purpose we use a further simplified charge model in which only the phosphate nodes (Fig. 1 *g*) carry charges. The precise value of the charges depends on the method used to calculate the solvation forces, as discussed below. The combination of different CM and CE models is summarized in Table 1.

The Debye-Hückel model

With the DH model, which is used in the OSF theory (31,32), charged sites without a finite size are embedded into the dielectric continuum of water. The implicit water and salt ions are everywhere and the dielectric constant is that of water in all space. The electrostatic interaction between two charged sites i and j with charge q_i and q_j is described as

$$U_{ij} = \frac{q_i q_j exp\left(-\kappa r_{ij}\right)}{\varepsilon r_{ij}}. \quad (3)$$

Here κ is the DH screening factor and proportional to $\sqrt{I}$, where I is the ionic strength or simply salt concentration c for monovalent salts such as NaCl. The value ε is the dielectric constant of water (78.0 at 298 K) and r_{ij} is the distance between the two charges. The corresponding electrostatic force can be evaluated by simplify differentiating U_{ij} with respect to the relevant coordinates. We note that the DH potential and force formula are analytical, and thus, there are no numerical errors involved.

To be consistent with the OSF theory, each phosphate group (or each phosphate node in the FEM representation, for both the polyion and molecular surface models) carries a charge of -0.24 *e*. This is based on the counterion condensation theory (39), which argues that the effective charge of the phosphate group is significantly neutralized by the condensed counterions by ~76% for a broad range of salt concentrations; there are also alternative explanations for the charge reduction (40).

The Poisson-Boltzmann solvation model

A much more sophisticated electrostatic model for solvation free energy and force is based on the PB theory (41), which has become popular in the biomolecular simulation community and shown to be accurate even at relatively high salt concentrations for monovalent ions (42) (also see Appendix 2). Compared to the DH model, the PB theory takes the dielectric boundary between the solute and solvent (and therefore solute shape) into consideration and is therefore expected to be much more reliable. Thanks to recent developments, PB equations can be solved for very large systems in an efficient manner (43,44).

In this work, the nonlinear PB solvation forces are calculated for the molecular surface FEM model for the DNA systems of interest. Since the effects of the counterions are explicitly considered in the nonlinear PB theory, the phosphate nodes bear the full charge of -1 instead of the screened value of -0.24 used in the DH model. To determine the dielectric boundary between DNA and the solvent, the Roux radii (45) are assigned to chemical nodes and each salt ion has a finite radius of 2.0 Å. The spline-based (46) molecular surface, which permits stable solvation force calculations, is used with a 0.3 Å spline window. The dielectric constants of DNA and solvent are set to be 1.0 and 80.0, respectively, which were also the values used in the parameterization of the Roux radii (45).

As discussed below, the nonlinear PB calculations for the solvation forces lead to convergence issues in the iterative CM/CE calculations. To evaluate the origin of the convergence issue, linear PB calculations are also carried out for the DNA models analyzed using the analytical DH theory. Specifically, -0.24 *e* charge is assigned to each phosphorus node and both chemical nodes and salt ions are assigned to a very small radius (0.01 Å); the dielectric constant is set to 78.0 in all space. In other words, these linear PB calculations effectively correspond to a numerical implementation of the DH model. By comparing the results to those using the analytical DH model, the effect of numerical errors in finite difference solution to the PB equation can be examined.

Throughout the article, we refer to the linear PB calculations using near-zero atomic radii and Manning charges ($-0.24e$ per phosphate) as PB1 calculations, and the nonlinear PB calculations using the realistic molecular shape and full phosphate charge ($-1.0e$) as PB2 calculations.

Salt concentration effects on DNA bendability: combining continuum mechanics and continuum electrostatics

To study the salt concentration effects on DNA bendability, it is necessary to incorporate CE into CM. DNA becomes stiffer at lower salt concentrations and therefore it is expected that the degree of bending is smaller at lower salt concentration under the same external force $\vec{F}_{ext}$. At a qualitative level, this is due to the larger electrostatic repulsive forces (or solvation forces) among phosphate groups at lower salt concentrations. To capture this effect explicitly, the differential solvation forces between different salt concentrations are integrated into the CM simulations that solve for DNA deformation under external force. Specifically, 0.15 M is chosen as the reference concentration since the corresponding Young's modulus values are known (see above); we note that the $E^{0.15}_{poly/mol}$ values estimated above are effective values that include contributions from both the intrinsic materials properties (i.e., at infinite salt concentration) and electrostatic solvation at 0.15 M. In other words, the effective free energy of the DNA (G^c_{tot}) at a given salt concentration, c, is given in the additive form

$$G^c_{tot} = G^{0.15}_{em} + G^c_{el} - G^{0.15}_{el}, \quad (4)$$

where $G^{0.15}_{em}$ is the elastic materials free energy evaluated at 0.15 M, and G^c_{el} is the electrostatic free energy at salt concentration, c.

Once the components of the CM/CE framework are specified as discussed above, the persistence lengths at different salt concentrations are extracted using two different protocols. One is forced-based and more generally applicable than the other. However, the other protocol is specific to the DNA bending problem, and is the protocol used here for validation, because of its apparent connection to the OSF theory (31,32). We note that the computational cost of the CM/CE calculations is very modest, especially when rather simple CE models (e.g., DH) are used; for most of the computations discussed in Results and Discussion, the cost is on the order of a few minutes on a single Linux machine.

The force-based protocol: the iterative CM/CE approach

In the first protocol, the structural deformation of the FEM models of DNA in response to an external bending force is explicitly calculated using the Calculix program (http://www.calculix.de/). The equilibrium (undeformed) structure is always taken as the straight B-form conformation and the bent structure is solved by static analysis under certain force loads and boundary conditions. Specifically, bending occurs in the x,z plane: the left end of the FEM model (~5% for the 36-bp and ~1% for the 300-bp) is fixed and a downwards (along the x axis) external force $\vec{F}_{ext}$ (summarized in Table 1) is applied at the right end as shown in Fig. 2 for the 36-bp molecular surface model; the degree of bending is exaggerated in the figure for clarity.

To explore explicitly the effect of salt concentration on DNA bendability, the differential solvation forces with respect to 0.15 M are applied to FEM models in addition to $\vec{F}_{ext}$ to solve for the structure of the deformed (bent) DNA. As illustrated in Fig. 3, this requires an iterative procedure that alternates between CM simulations and solvation force calculations:

Step 1. $\vec{F}_{ext}$ is applied to the straight structure and a deformed (bent) conformation is obtained by finite element analysis.

Step 2. The positions of all chemical nodes of DNA are extracted from the bent mesh and solvation forces are calculated at salt concentration c relative to 0.15 M (see Solvation force calculations: continuum electrostatics). The differential solvation forces are calculated as: $\vec{F}_{diff} = \vec{F}_c - \vec{F}_{0.15M}$.

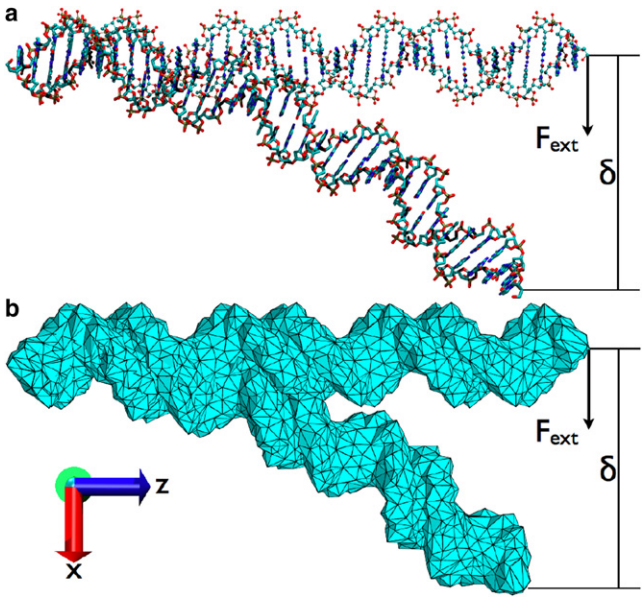

FIGURE 2 A scheme that illustrates the bending of a 36-bp DNA in the x,z plane by an external force $\vec{F}_{ext}$ at the right terminus for the evaluation of DNA bendability with a force-based CM/CE protocol. The displacement δ at the right terminus in the x direction is also shown. (*a*) Heavy atoms (chemical nodes) shown in CPK and licorice for the straight and bent structures, respectively. (*b*) Straight and bent structures shown in mesh. The magnitude of bending is exaggerated for clarity. See Table 1 for the magnitude of the forces applied in real CM/CE simulations.

Step 3. The differential solvation forces on the phosphorus nodes are included in the FEM simulations as force loads in addition to $\vec{F}_{ext}$ and a new deformed structure is obtained.

Step 4. Several iterations of Steps 2–4 are carried out until the deformed structure is converged, which indicates that $\vec{F}_{ext}$ plus the differential solvation forces are in equilibrium with the internal materials forces due to deformation.

To extract the value of the persistence length from the converged bent conformation, one might use the inverse linear relationship between the displacement of the DNA's right terminus (see Fig. 2), δ, and the Young's modulus at a given salt concentration, E^c,

$$\delta = F_{ext}L^3/3E^cJ, \tag{5}$$

where F_{ext} is the magnitude of the applied force load, L is the contour length, and J is the moment of inertia of cross section. Once δ is measured from the converged bent conformation, E^c can be calculated based on Eq. 5, which in turn gives the corresponding persistence length following Eq. 2. However, we note that Eq. 5 rigorously holds only for very small degrees of bending, which may not be the case in our simulations. Therefore, we chose an alternative scheme in which, for each CM/CE simulation, we carry out a reference CM simulation (with the corresponding FEM model at the reference 0.15 M salt concentration) to obtain the explicit numerical relationship between δ and $1/E^c$ under the same external force $\vec{F}_{ext}$. This numerical relationship is then used to convert the measured δ in the converged bent DNA into the corresponding E^c and persistence length at other salt concentrations.

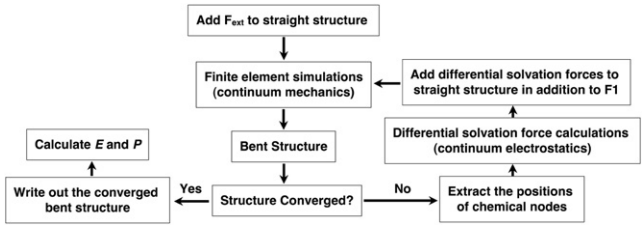

FIGURE 3 The flow chart for the force-based CM/CE calculation for DNA bending.

The energy-based protocol: validation of the CM/CE framework

In both the OSF theory (31,32) and recent numerical studies (35), an energy-based approach was used to extract the salt concentration dependence of DNA persistence length. These calculations assume a uniform bending of DNA and therefore a constant radius of curvature R along the DNA contour. Under these assumptions, given the phosphorus coordinates (x, y, z) of the straight DNA, the phosphorus coordinates (x', y', z') in a bent DNA in the x,z plane can be obtained analytically (35) as

$$x' = (R + x)\cos\theta y' = y\,z' = (R + x)\sin\theta, \tag{6}$$

where R is the radius of curvature, $\theta = z/R$. The electrostatic free energy can then be calculated for both straight and bent DNA, giving the bending electrostatic free energy of

$$\Delta G_{el} = G_{el}(bent) - G_{el}(straight). \tag{7}$$

Using a simple DH model for charge-charge interactions, we found that ΔG_{el} follows a linear relationship with $1/R^2$,

$$\Delta G_{el} = P_{el}k_BTL/2R^2, \tag{8}$$

where P_{el} is the electrostatic contribution to the persistence length and L is the contour length. Therefore, P_{el} can be obtained from the slope of ΔG_{el} versus $1/R^2$ and the total persistence length is given as

$$P = P_o + P_{el}, \tag{9}$$

where P_o is typically chosen such that P is 500 Å at 0.15 M. Throughout the article, we refer to this procedure of displacing only the phosphorus (charged) sites as the energy-based calculation and use it to compare with the more general CM/CE simulations that involve explicit DNA deformation under external force.

RESULTS AND DISCUSSION

Considering the intrinsic additive nature of this model regarding the materials (elastic) and electrostatic contributions to bendability, a useful reference of comparison is the result of the OSF theory (31,32), which was developed for an infinitely long polyion model of DNA; it predicts that $P_{el} = 0.324/c$ Å. In reality, the treatment of DNA as infinitely long may not be justified, especially at low salt concentration where the DH screening length, κ^{-1}, is large. Therefore, we have also tested an extension of the original OSF theory that considers the electrostatic end-effects explicitly (34). As shown in Appendix 1, the modified OSF prediction can be cast in a similar functional form $P_{el} = 0.324/c'$ Å, where the effective salt concentration c' depends on both κ and the DNA contour length, L,

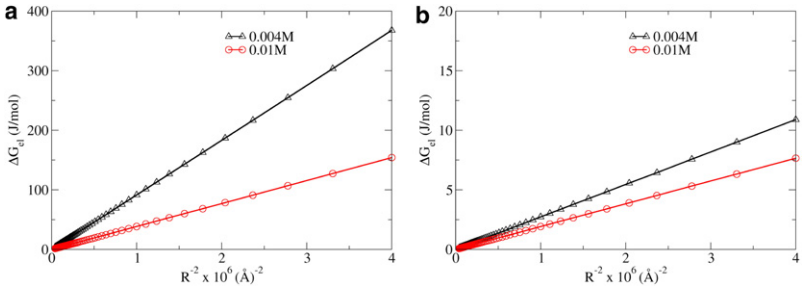

FIGURE 4 ΔG_{el} (Eqs. 7 and 8) versus $1/R^{-2}$ for (*a*) a 300-bp and (*b*) a 36-bp polyion DNA at 0.004 M and 0.01 M NaCl.

$$c' = \frac{c}{\left\{1 + e^{-\kappa L}\left(\frac{\kappa L}{3} + \frac{8}{3\kappa L} + \frac{5}{3}\right) - \frac{8}{3\kappa L}\right\}}. \quad (10)$$

We note that as $L >> \kappa^{-1}$, $c' \rightarrow c$ and the original OSF result is recovered.

Linear inverse *c* dependence of *P* for 300-bp DNA

As shown in Fig. 4 *a*, the bending electrostatic energy ΔG_{el} for a uniformly bent polyion DNA varies linearly as the inverse square of the radius of curvature using the DH model for electrostatics, in agreement with previous studies (35). The extracted persistence length, at different salt concentrations following Eq. 8, agrees well with the OSF prediction. As summarized graphically in Fig. 5 *a* and numerically in Table 2, the persistence length scales linearly as a function of the inverse concentration, in agreement with the OSF prediction (31,32). The slight difference (<2% at 0.004 M) is because a finite DNA (300 bp) is used in these simulations while OSF assumes an infinitely long DNA. Nevertheless, the DH screening length even at the lowest concentration considered here (0.004 M) is ~48 Å, far smaller than the contour length (~1020 Å) of the DNA model, thus the electrostatic end-effect (35) is not significant (also see Appendix 1). With the molecular surface model and the DH treatment of electrostatics, very similar persistence lengths are obtained from the energy-based analysis; the largest deviation observed is <2%. Therefore, the double-helical pattern of phosphate distribution does not seem to have a major effect on the long-range materials' property (persistence length) of DNA, confirming the physical relevance of the OSF theory.

With the force-based protocol, which explicitly solves for the deformation of DNA under external force in the combined CM/CE framework, the results using the DH electrostatic treatment are generally consistent with that from the energy-based analysis and therefore the OSF prediction; this is true regardless of the FEM models (polyion versus molecular surface) for the DNA. The linear dependence of the persistence length on the inverse salt concentration is well-reproduced (Fig. 5 *b*). Regarding the absolute values of the persistence length, the largest deviation from OSF is observed at very low salt concentration; at 0.004 M, for example, the difference between the force-based result and OSF is ~30 Å with the polyion model and ~25 Å with the molecular surface model (Table 2).

A disappointing finding is that convergence of the force-based protocol cannot be reached when electrostatics are treated using the more sophisticated PB theory, regardless of the FEM model for the DNA and charges for the phosphate. That is, although both the PB and the FEM calculations converge fine by themselves, the predicted bent conformation of DNA fluctuates significantly during the CM/CE iteration (Fig. 3), which prevents a meaningful persistence length from being extracted. Another example: with $|F_{ext}| =$ 0.003 pN, the predicted displacement of the right terminus varies ~10–30 Å during the CM/CE iteration, which is substantially larger than the expected difference in displacement at different salt concentrations. Comparing the forces from PB1 and DH calculations indicates that this is likely due to the numerical errors in the finite difference PB calculations. Although the difference is small (~0.01 pN) by the standard of most applications, it is significant in this context due to the fact that a very small force is required to bend the 300-bp DNA (tested $|F_{ext}|$ ranges from 0.003 pN to 0.03 pN, which causes the right terminus to displace between ~30 and 300 Å). This sensitivity toward small numerical noise in the solvation force persists under different deformation modes

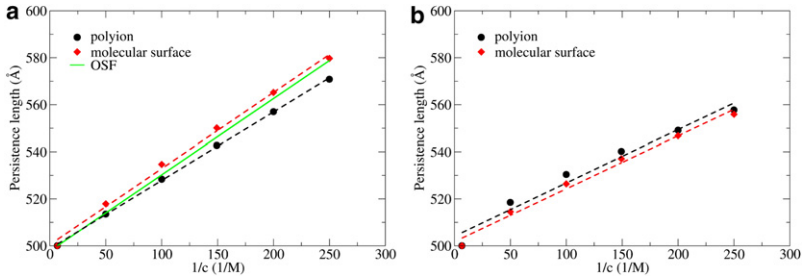

FIGURE 5 Predicted persistence length (*P*) versus $1/c$ for the polyion and molecular surface models of the 300-bp DNA from (*a*) energy-based calculations and (*b*) force-based CM/CE simulations. The DH model is used for the electrostatic interactions in all calculations. The dashed lines represent linear fitting and all correlation coefficients are >0.98. The solid line represents the prediction from the OSF theory.

TABLE 2 Predicted persistence length (*P*) at different salt concentrations (*c*) for a 300-bp DNA

c (M)	1/*c* (1/M)	*P* (Å) Polyion CM/CE	*P* (Å) Polyion energy	*P* (Å) Molecular surface CM/CE	*P* (Å) Molecular surface energy	*P* (Å) OSF
0.004	250.0	557.7	570.8	555.9	579.7	578.8
0.005	200.0	549.1	557.0	546.8	565.2	546.2
0.0067	149.3	540.2	542.7	537.1	550.1	562.6
0.01	100.0	530.4	528.4	526.4	534.7	530.2
0.02	50.0	518.5	513.5	514.5	517.9	514.0
0.15	6.7	500.0	500.0	500.0	500.0	500.0

The reference value of *P* is 500.0 Å at 0.15 M. Unless otherwise indicated, the Debye-Hückel model is used for the electrostatic interactions.

TABLE 3 Predicted persistence length (*P*) at different salt concentrations (*c*) for a 36-bp DNA

c (M)	1/*c*′* (1/M)	*P* (Å) Polyion CM/CE	*P* (Å) Polyion energy	*P* (Å) Molecular surface CM/CE(DH)	*P* (Å) Molecular surface CM/CE(PB)	*P* (Å) Molecular surface energy
0.004	54.6	518.8	516.9	518.1	513.3	520.8
0.006	47.8	517.1	514.5	516.1	511.4	518.2
0.01	38.6	514.5	511.3	513.3	509.1	514.6
0.03	20.2	508.5	505.0	506.9	505.9	507.1
0.05	13.8	505.7	502.8	504.2	504.8	504.2
0.1	7.8	502.1	500.8	501.2	502.3	501.3
0.15	5.5	500.0	500.0	500.0	500.0	500.0

The reference value of *P* is 500.0 Å at 0.15 M. Unless otherwise indicated, the Debye-Hückel (DH) model is used for the electrostatic interactions.
*The effective salt concentration according to the modified OSF theory (see Appendix 1).

(e.g., four-point flexure), which is likely due to the high symmetry of the DNA system. Whether the numerical problem becomes less significant for shorter DNAs will be studied below using the much shorter 36-bp DNA.

Linear inverse *c*′ dependence of *P* for 36-bp DNA

For the 36-bp DNA, when the DH model is used for electrostatics, the bending electrostatic energy still scales well with respect to the inverse square of the uniform bending curvature (Fig. 4 *b*). A qualitative difference compared to the 300-bp DNA is, at low salt concentration, that the DH screening length (~48 Å for 0.004 M) becomes comparable to the counterlength (~120 Å). Therefore, the electrostatic end effect becomes significant at low salt concentration. Indeed, comparing Tables 2 and 3, at 0.004 M, for example, the predicted persistence lengths for the 36-bp and 300-bp DNAs differ by ~50 Å (i.e., ~10%) regardless of the FEM model and evaluation protocol (i.e., energy versus force-based CM/CE). Moreover, the persistence length does not show a linear relationship with 1/*c* as for the 300-bp case (see Fig. 6, *a* and *b*). Rather, the results of both energy-based and force-based evaluations (Fig. 6, *c* and *d*) scale inversely with the effective salt concentration, c' (Eq. 10), as predicted by the modified OSF theory (34, see also Appendix 1). Similar to the 300-bp case, the results are very similar with either the polyion or molecular surface FEM models; the largest difference is only a few Ångstroms even at very low (e.g., 0.004 M) salt concentrations.

Regarding the effect of numerical noises in the finite difference PB force calculations, it is possible that the impact is smaller for the 36-bp DNA compared to the 300-bp case since a much larger external force ($|F_{ext}|$ ~0.4 pN) is needed to induce the similar degree of bending. Indeed, with the molecular surface model and PB1 calculations for the electrostatics, although the magnitude-of-force noise compared to the analytical DH force is still ~0.01 pN (see Fig. 7), convergence in the CM/CE simulations can be reached and the extracted persistence lengths at different salt concentrations agree well with the DH results (see Fig. 6 *b* and Table 3). With

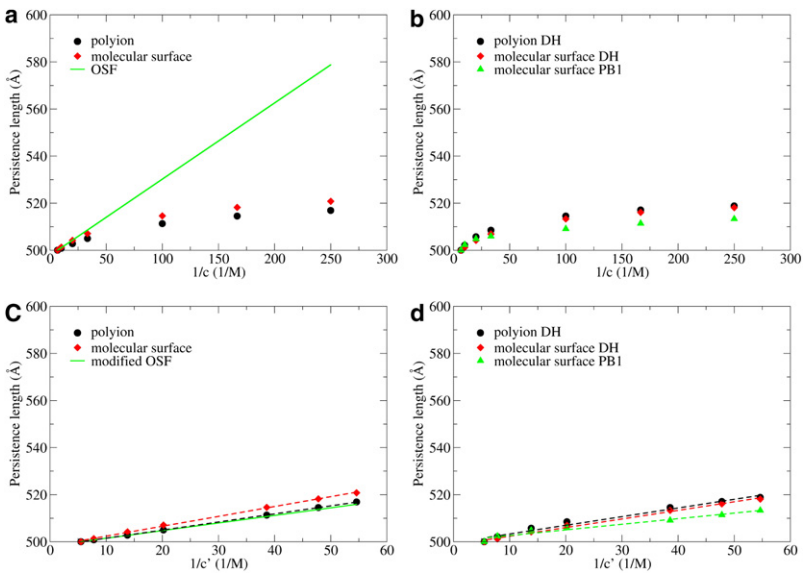

FIGURE 6 The relationship between predicted persistence length (*P*) and salt concentration for the 36-bp DNA. In panels *a* and *b*, the numerical simulations are compared to the original OSF theory and therefore *P* is plotted against the inverse salt concentration; in panels *c* and *d*, the comparison is made to the modified OSF theory (see Appendix 1), and *P* is plotted against the inverse of the effective salt concentration (Eq. 10). As in Fig. 5, the numerical results from both energy- and force-based analyses are given; the dashed lines in panels *c* and *d* represent linear fitting and all correlation coefficients are >0.98. The solid line represents prediction from the original OSF theory in panel *a* and modified OSF in panel *c*.

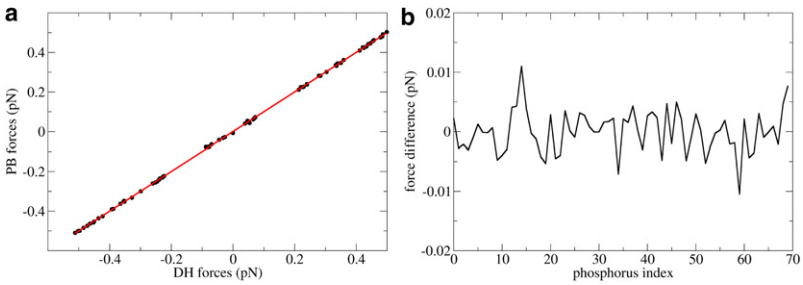

FIGURE 7 Comparison of PB and DH differential solvation forces at 0.004 M (relative to 0.15 M) for an arbitrary bent structure of molecular surface model of 36-bp DNA; to facilitate the comparison, the PB1 model is used (see Solvation force calculations: continuum electrostatics for details). (*a*) A direct comparison of forces; (*b*) the difference of forces at the two different levels for phosphorus nodes.

the more sophisticated PB2 setup, unfortunately, even larger numerical noises are found in the calculated solvation force, which again lead to convergence failure in the iterative CM/CE simulations; this is independent of whether the full charge or the reduced charge (39,40) is used. As shown in the Appendix 2, PB2 calculations with the full charge in fact lead to forces in close agreement with microscopic Monte Carlo simulations of the counterions. Therefore, the convergence issue of the iterative CM/CE protocol arises not from any unphysical nature of the PB theory; instead, it is from the similar magnitudes of the numerical noise in the PB force and the external force required for the small deformation of a highly symmetric system.

Comparison to previous studies: strengths and limitations of the combined CM/CE framework

Before comparing the results of the CM/CE simulations with available experimental and theoretical studies in the literature, we note that the salt dependence of DNA bendability is a subject of long history and remains an active topic of discussion to this day. The goal of this work is not to resolve the existing controversies (see, for example, discussions in (33)), which may require more sophisticated models for DNA than adopted here. Rather, the goal is to use a sufficiently realistic representation of DNA to explore the numerical performance and stability of the combined CM/CE framework. Indeed, the current model implicitly assumes an additive nature regarding the contributions from elastic and electrostatic factors to the persistence length, which makes it most sensible to use the OSF theory (31, 32) and its extension (34) as the reference for comparison, despite the limitations of the theory as discussed in the literature (33).

For the salt concentration dependence of DNA bendability, results obtained for the 300-bp DNA using the CM/CE framework are consistent with OSF theory (31,32) and recent single molecule stretching experiments at both qualitative and quantitative levels (22,24). Qualitatively, the inversely linear relationship between the persistence length and salt concentration is well reproduced. Quantitatively, the CM/CE framework shows that the persistence length increases from 50 nm to ~56 nm when the salt concentration is decreased from 0.15 M to 0.004 M, in good agreement with recent single molecule experiments (24), which measured that the persistence length increased from ~45 $\pm$ 2 nm to 58 $\pm$ 2 nm for the same range of salt concentrations. Since a rather crude model of DNA is applied in this study, this level of agreement indicates that fine molecular details (e.g., detailed distribution of atomic charges) are not essential to the large-scale behavior of a single DNA molecule. Computationally, Bomble and Case (47) explored the salt-concentration dependence of DNA flexibility using all-atom normal mode analysis and the Generalized Born model for solvation (48); the salt screening term in their Generalized Born model is the DH potential (49). The persistence length was extracted by comparing the normal mode results to those from an elastic rod model. Due to the computational cost of all-atom normal mode analysis, calculations were primarily carried out for a 60-bp DNA. Nevertheless, their calculations qualitatively reproduced the salt concentration dependence of the persistence length found in single molecule experiments (22), although the deviation was ~10 nm, somewhat larger that those found in this study. It is convenient to consider sequence dependence of DNA bendability with this model, although it remains computationally too intense for large systems.

In the broader context of biomolecular simulations of DNA or protein/DNA complexes at large length scale, there are several previous studies that modeled DNA mechanical deformation using either finite element analysis (26–28) or analytical elasticity theory (30,50), as summarized in a recent review article (29). In these studies, DNA molecule is modeled as an elastic cylindrical rod with either homogeneous or sequence-dependent materials' property and the anisotropy of bending rigidity has also been taken into account (28,29). These works have provided meaningful insight regarding DNA deformations at either a local scale, such as local bending by proteins (28,29), or a global scale, such as DNA looping (19,50,51) or supercoiling (26). Compared to these studies, our molecular surface model can take into account the molecular shape of the DNA molecule. Although this is found not to be crucial for the simple DNA bending problem analyzed here, going beyond a simple rod model can be particularly helpful in cases where the molecular nature of the protein-DNA interface (7,19,51–53) is important. Meanwhile, although not implemented in this study, the sequence and/or direction dependence of

materials' property can be incorporated into the molecular surface model if needed. More importantly, our CM/CE framework treats electrostatic interactions explicitly, which enables its application to DNA bending by proteins through electrostatic forces or the mechanical deformation of DNA at different salt concentrations, as analyzed in this study. Along this line, the finding that the most sophisticated PB treatment of electrostatics leads to numerical convergence problems in the iterative CM/CE protocol is somewhat disappointing and underlines the importance of carefully balancing the numerical accuracy of different approaches when dealing with a problem that involves multiple length scales (e.g., few Ångstroms vs. 0.1 μm for the 300-bp DNA). However, we also emphasize that this numerical problem is likely rather specific to this system, which has a high degree of spatial symmetry and huge anisotropy in shape. As a result, a very small amount of external force (e.g., ~0.003 pN for the 300-bp DNA) is required to bend one end of the DNA, and small numerical noises in the PB forces (~0.01 pN) become important. In most biomechanical processes, the force involved is typically on the order of a few to tens of pN (10,54,55), for which the noises of ~0.01 pN in the PB forces are likely much less significant. Therefore, the applicability of the PB approach, which is much more versatile than the simple DH model, deserves further careful analysis with other biomechanical problems. The molecular surface representation is also advantageous when studying processes that involve a significant change in the solvent-accessible surface during the conformational transition, such as the MscL gating transition (56) that motivated our study.

Finally, we note that the pioneering studies of Villa et al. (30) and Balaeff et al. (50,57) combined the elastic model of DNA and atomistic model of *lac* repressor in a multiscale framework, where the electrostatic interaction involving the elastic DNA was modeled using a DH potential. In principle, our combined CM/CE framework can be extended in a similar fashion to include atomistic models for some components; using the finite element representation instead of an elastic rod model offers more flexibility, especially near the interface between the atomistic and CM components. In this context, the molecular surface representation makes it possible to encode the chemical characteristics (e.g., charge, radii and van der Waals parameters) with the chemical nodes such that both solvation and interactions between different components can be computed in a straightforward fashion.

CONCLUSIONS

As a useful step toward developing a quantitative theoretical framework based on CM models of biomolecules, we have developed a computational protocol that effectively incorporates CE in CM calculations. The combined CM/CE protocol allows straightforward encoding of the most essential chemical characteristics (e.g., charge distribution) and energetic features (e.g., solvation) of the system when studying the structural response of biomolecules or biomolecular assemblies to external mechanical perturbations. The use of the flexible finite element representation and simulation makes the CM/CE protocol generally applicable to biomolecular systems of arbitrary shape and mechanical perturbations of complex forms and large length scales.

As the first application, the combined CM/CE protocol is used to study the salt concentration dependence of DNA bendability based on a framework consistent with the fundamental assumptions of the OSF theory (31, 32, 34) (i.e., the electrostatic and materials contributions to persistence length are additive). To explore the numerical stability of the protocol, two different CM models for the DNA (polyion and molecular surface models) and two electrostatic models (DH and PB) have been studied for two DNA systems of variable lengths (36 bp and 300 bp). The bendability (characterized by persistence length) of the DNA is analyzed as a function of salt concentration using 0.15 M NaCl as the reference. The CM/CE simulations that employ an external force to study explicitly the DNA deformation, which is a generally applicable protocol, lead to results consistent with an energy-based analysis uniquely suitable for the uniform bending of DNA. Both types of numerical analyses are in good agreement (in terms of salt concentration dependence) with predictions from the original OSF theory and available experimental data. For the very short DNA (36 bp) at very low salt concentration, a modified OSF theory that explicitly considers the end effects has been found to better capture the numerical simulation results. A somewhat alarming result found in this study is that the CM/CE calculations are plagued with convergence issues when the more sophisticated PB model is used to describe electrostatics, which is likely due to the fact that these DNA systems, especially the 300-bp one, are highly anisotropic and therefore the predicted mechanical behavior is particularly sensitive to small numerical noise in the PB forces. Although we do not anticipate this as a serious challenge to general CM/CE applications, the finding highlights the importance of balancing numerical accuracy of the CM and CE models. For example, although the DH model is much simpler than PB, it can be parameterized based on PB (58) and its analytical nature makes it particularly attractive for application to very large biomolecules.

In summary, although further developments in parameterizing heterogeneous CM models for complex biomolecules and establishing numerically efficient and stable CE models are required to make combined CM/CE simulations predictive in nature, this intrinsically multiscale computational framework is particularly promising for exploring the mechanisms of cellular processes that involve large length scales, such as mechanosensation, cell motility, and transcription regulation.

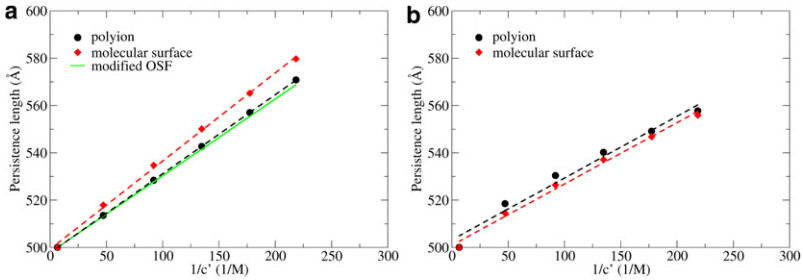

FIGURE 8 Same as Fig. 5 in the main text (for the 300-bp DNA), except that the results are plotted against the inverse of the effective salt concentration in the modified OSF theory. Note the better agreement between the energy-based numerical calculation using the polyion model and the modified OSF prediction compared to the original OSF prediction (Fig. 5 *a*) even for the relatively long (300-bp) DNA.

APPENDIX 1: AN EXTENSION TO THE OSF THEORY TO TREAT ELECTROSTATIC END EFFECTS

The OSF theory (31,32) was originally developed for an infinitely long polyion model of DNA. Since the DH screening length at 0.004 M is comparable to the contour length of a 36-bp DNA, the electrostatic end-effects become significant and therefore the relationship between P and c should not follow the prediction of the original OSF theory, as found in the calculations discussed in the main text. This is explicitly illustrated in Fig. 6, *a* and *b*, which highlight that a revision of the OSF theory is clearly necessary for short DNAs. This has been accomplished by Hagerman in (34), which unfortunately contains several rather important typographical errors in key equations. Therefore, in this Appendix, we rederive the extension to the original OSF theory in detail and present the result in the form of the OSF expression but with an effective salt concentration. We follow the derivation of the original OSF theory for a rod with continuous charge distribution and the notations used are consistent with Skolnick and Fixman (32).

Given a rod with continuous charge distribution, the change of electrostatic potential at a reference point along the contour of the rod due to uniform bending is given by Eq. II.14 of Skolnick and Fixman (32),

$$V^* = \frac{\sigma_0}{D}\left[\int_0^{L_1}\left\{\frac{e^{-\kappa|F(s)|}}{|F(s)|}-\frac{e^{-\kappa s}}{s}\right\}ds+\int_0^{L_2}\left\{\frac{e^{-\kappa|F(s)|}}{|F(s)|}-\frac{e^{-\kappa s}}{s}\right\}ds\right]. \tag{11}$$

Here σ_0 is the charge per unit length; κ is the DH screening length; D is the solvent dielectric constant; s is the arc length from the reference point to any point along the rod; L_1 and L_2 are the arc lengths from the reference point to the left and right ends of the rod, respectively; and $|F(s)|$ is the spatial distance in the bent configuration between the reference point to any point. The two integrals in Eq. 11 are very similar and we define one of them as V_1,

$$V_1 = \frac{\sigma_0}{D}\int_0^{L_1}\left\{\frac{e^{-\kappa|F(s)|}}{|F(s)|}-\frac{e^{-\kappa s}}{s}\right\}ds. \tag{12}$$

Following Skolnick and Fixman (32),

$$\frac{e^{-\kappa|F(s)|}}{|F(s)|} = e^{-\kappa s}\left\{\frac{1}{s}+\frac{s}{24R_c^2(0)}+\frac{\kappa s^2}{24R_c^2(0)}\right\}, \tag{13}$$

where $R_c(0)$ is the radius of curvature in uniform bending. Substituting Eq. 13 into Eq. 12 leads to

$$V_1 = \frac{\sigma_0}{24DR_c^2(0)}\left\{\int_0^{L_1}e^{-ks}sds+\int_0^{L_1}e^{-ks}\kappa s^2ds\right\}, \tag{14}$$

which can be further simplified via integration by parts,

$$V_1 = \frac{\sigma_0}{24DR_c^2(0)}\left\{\frac{3}{\kappa^2}-\frac{1}{\kappa^2}e^{-\kappa L_1}\left(\kappa^2L_1^2+3\kappa L_1+3\right)\right\}. \tag{15}$$

For infinitely long DNA, $L_1 \to \infty$ or for $L_1 >> \kappa^{-1}$, V_1 reaches the upper limit as

$$V_1^{\infty} = \frac{\sigma_0}{8D\kappa^2R_c^2(0)}. \tag{16}$$

This is the result of the original OSF theory and P_{el} (the electrostatic contribution to P) can be obtained from the slope between $V_1{}^{\infty}$ and $1/R_c{}^2(0)$ and is proportional to $1/\kappa^2$ or $1/c$. Substitution in the relevant parameters leads to the familiar OSF equation:

$$P_{el} = 0.324/c\text{Å}. \tag{17}$$

For a DNA of finite length, V_1 can be explicitly calculated according to Eq. 15. Moreover, V_1 is position-dependent and therefore it is useful to compute the average value of V_1 over the contour length L,

$$V_1^{avg} = \frac{\int_0^{L_1}V_1dL_1}{\int_0^{L_1}dL_1}. \tag{18}$$

Integrating by parts leads to

$$V_1^{avg} = \frac{\sigma_0}{8D\kappa^2R_c^2(0)}\left\{1+e^{-\kappa L}\left(\frac{\kappa L}{3}+\frac{8}{3\kappa L}+\frac{5}{3}\right)-\frac{8}{3\kappa L}\right\}. \tag{19}$$

Therefore, P_{el} should be proportional to

$$\frac{1}{\kappa^2}\left\{1+e^{-\kappa L}\left(\frac{\kappa L}{3}+\frac{8}{3\kappa L}+\frac{5}{3}\right)-\frac{8}{3\kappa L}\right\}, \tag{20}$$

or more explicitly,

$$P_{el} = 0.324\frac{1}{c}\left\{1+e^{-\kappa L}\left(\frac{\kappa L}{3}+\frac{8}{3\kappa L}+\frac{5}{3}\right)-\frac{8}{3\kappa L}\right\}. \tag{21}$$

If we define c' as

$$c' = \frac{c}{\left\{1+e^{-\kappa L}\left(\frac{\kappa L}{3}+\frac{8}{3\kappa L}+\frac{5}{3}\right)-\frac{8}{3\kappa L}\right\}}, \tag{22}$$

which has the same unit as c and can be regarded as an effective salt concentration, Eq. 21 can be arranged in the form of the original OSF theory with c replaced by c',

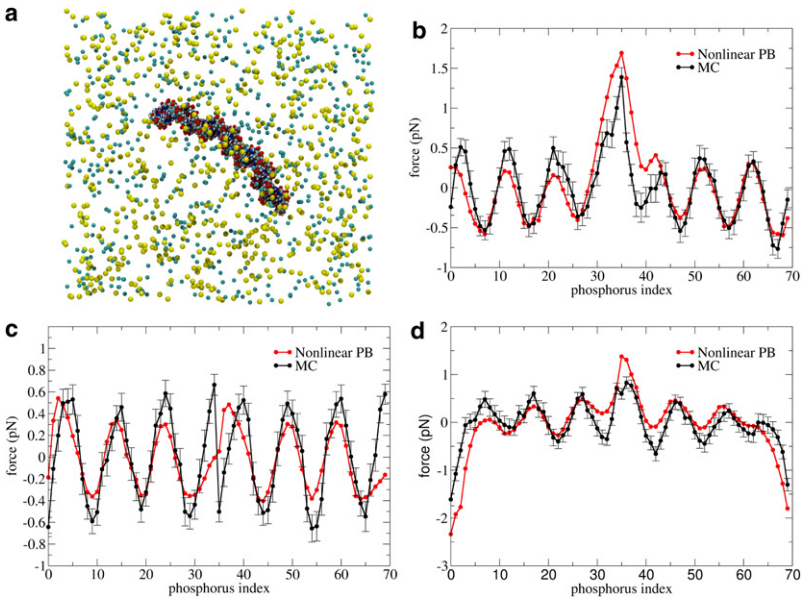

FIGURE 9 Comparison of differential solvation force (0.03 M relative to 0.15 M NaCl) calculated using explicit ions and PB theory for a bend structure of a 36-bp DNA. The explicit ion result is based on Monte Carlo simulations (see text). The setup of the PB calculations is described in the main text (PB2 in Solvation force calculations: continuum electrostatics). (*a*) A snapshot from the MC Simulation at 0.15 M NaCl. The DNA is shown in the van der Waals scheme; sodium and chloride ions are shown in yellow and cyan, respectively. (*b*) Comparison of the *x* component of differential solvation forces. (*c*) Comparison of the *y* component of differential solvation forces. (*d*) Comparison of the *z* component of differential solvation forces.

$$P_{\mathrm{el}} = 0.324/c'\text{Å}. \tag{23}$$

For infinitely long DNA or $L_1 >> \kappa^{-1}$, the result reduces to the original OSF prediction.

As shown in Fig. 8, even with a 300-bp DNA, the modified OSF theory seems to agree better with the energy-based numerical calculation than the original OSF prediction (Fig. 5 *a*). For the shorter 36-bp DNA, the modified OSF agrees well with numerical simulations (Fig. 6).

APPENDIX 2: VALIDATION OF NONLINEAR POISSON-BOLTZMANN FOR BENT DNA USING MONTE CARLO SIMULATIONS

To evaluate the accuracy of PB2 solvation forces, especially concerning the effect of neglecting ion-ion correlation in the PB theory (41), we compare the PB2 force with Monte Carlo simulations in which the ions are treated explicitly. The accuracy of PB for DNA in the straight conformation has been evaluated in previous studies (see (42)), but no such comparison has been made for a bent conformation. An arbitrary bent structure of the 36-bp DNA is chosen and an all-atom model is built using the Hbuild module in CHARMM (59). Periodic boundary condition with a rectangular box is applied and the box size is set by leaving 60 Å on all sides in three directions; the final box is 199 Å × 147 Å × 220 Å. Two systems with NaCl concentration of 0.15 M (Fig. 9 *a*) and 0.03 M are studied, which contain 651 sodium, 581 chloride ions and 186 sodium, 116 chloride ions, respectively. During the simulation, the DNA molecule is fixed in space and only the ions are allowed to move. The dielectric constant is set to 78.0 throughout the space, with a cutoff for electrostatic interactions of 50.0 Å. The attractive components of all van der Waals interactions are turned off. In this way, we are mimicking the CE model with salt ions treated explicitly. The ion distribution around the DNA is sampled using Metropolis Monte Carlo with simple translational moves. The maximum translation step size is set to 5.0 Å and $>10^5$ sweeps are performed for each system; each sweep corresponds to a reshuffling of all salt ions. To calculate solvation forces, for each saved snapshot, the electrostatic force on each phosphorus atom of DNA due to other phosphorus atoms and salt ions is calculated. The averaged solvation force on each phosphorus atom is then calculated by averaging over the entire MC trajectory. The same procedure is carried out for two systems and the differential solvation forces are compared to the PB2 result: $\vec{F}_{\mathrm{diff}} = \vec{F}_{0.03\mathrm{M}} - \vec{F}_{0.15\mathrm{M}}$. The uncertainty of forces are evaluated using the standard block average method (60).

As shown in Fig. 9, the PB2 forces agree rather well with the Monte Carlo results in all directions. Therefore, the PB theory is physically sound for the current purpose of looking at DNA deformation at different salt concentrations. This confirms that the convergence issue encountered in the iterative CM/CE simulations is purely numerical in nature.

L.M. thanks Dr. Yuye Tang for help with FEM simulations. Computational resources from the National Center for Supercomputing Applications at the University of Illinois are greatly appreciated.

The research has been supported from the National Institutes of Health (grant No. R01-GM071428). Q.C. also acknowledges a Research Fellowship from the Alfred P. Sloan Foundation.

REFERENCES

1. Alberts, B., D. Bray, J. Lewis, M. Raff, K. Roberts, et al. 1994. Molecular Biology of the Cell. Garland Publishing, New York.
2. Geeves, M. A., and K. C. Holmes. 1999. Structural mechanism of muscle contraction. *Annu. Rev. Biochem.* 68:687–728.
3. Geeves, M. A., and K. C. Holmes. 2005. The molecular mechanism of muscle contraction. *Adv. Protein Chem.* 71:161–193.
4. Wigley, D. B. 1995. Structure and mechanism of DNA topoisomerases. *Annu. Rev. Biophys. Biomol. Struct.* 24:185–208.
5. Vologodskii, A. V., and N. R. Cozzarelli. 1994. Conformational and thermodynamic properties of supercoiled DNA. *Annu. Rev. Biophys. Biomol. Struct.* 23:609–643.
6. Schleif, R. 1992. DNA looping. *Annu. Rev. Biochem.* 61:199–223.
7. Swinger, K. K., and P. A. Rice. 2004. IHF and HU: flexible architects of bent DNA. *Curr. Opin. Struct. Biol.* 14:28–35.
8. Martinac, B. 2004. Mechanosensitive ion channels: molecules of mechanotransduction. *J. Cell Sci.* 117:2449–2460.
9. Perozo, E. 2006. Gating prokaryotic mechanosensitive channels. *Nat. Rev. Mol. Cell Biol.* 7:109–119.
10. Zhu, C., G. Bao, and N. Wang. 2000. Cell mechanics: mechanical response, cell adhesion, and molecular deformation. *Annu. Rev. Biomed. Eng.* 2:189–226.
11. Tang, Y. Y., G. X. Cao, X. Chen, J. Yoo, A. Yethiraj, et al. 2006. A finite element framework for studying the mechanical response of

macromolecules: application to the gating of the mechanosensitive channel MscL. *Biophys. J.* 91:1248–1263.

12. Chen, X., Q. Cui, Y. Y. Tang, J. Yoo, and A. Yethiraj. 2008. Gating mechanisms of mechanosensitive channels of large conductance. I: A continuum mechanics-based hierarchical framework. *Biophys. J.* 95:563–580.
13. Tang, Y. Y., J. Yoo, A. Yethiraj, Q. Cui, and X. Chen. 2008. Gating mechanisms of mechanosensitive channels of large conductance. II: Systematic study of conformational transitions. *Biophys. J.* 95:581–596.
14. Tang, Y., J. Yoo, A. Yethiraj, Q. Cui, and X. Chen. 2008. Mechanosensitive channels: insights from continuum-based simulations. *Cell Biophys. Biochem., In press.*
15. Davis, M. E., and J. A. McCammon. 1990. Electrostatics in biomolecular structure and dynamics. *Chem. Rev.* 90:509–521.
16. Honig, B., and A. Nicholls. 1995. Classical electrostatics in biology and chemistry. *Science.* 268:1144–1149.
17. Feig, M., and C. L. Brooks, III. 2004. Recent advances in the development and application of implicit solvent models in biomolecule simulations. *Curr. Opin. Struct. Biol.* 14:217–224.
18. Baker, N. A. 2005. Improving implicit solvent simulations: a Poisson-centric view. *Curr. Opin. Struct. Biol.* 15:137–143.
19. Vilar, J. M. G., and L. Saiz. 2005. DNA looping in gene regulation: from the assembly of macromolecular complexes to the control of transcriptional noise. *Curr. Opin. Gene. Dev.* 15:136–144.
20. Eisenberg, H. 1987. DNA flexing, folding, and function. *Acc. Chem. Res.* 20:276–282.
21. Hagerman, P. J. 1988. Flexibility of DNA. *Annu. Rev. Biophys. Biophys. Chem.* 17:265–286.
22. Baumann, C. G., S. B. Smith, V. A. Bloomfield, and C. Bustamante. 1997. Ionic effects on the elasticity of single DNA molecules. *Proc. Natl. Acad. Sci. USA.* 94:6185–6190.
23. Bustamante, C., Z. Bryant, and S. B. Smith. 2003. Ten years of tension: single-molecule DNA mechanics. *Nature.* 421:423–427.
24. Wenner, J. R., M. C. Williams, I. Rouzina, and V. A. Bloomfield. 2002. Salt dependence of the elasticity and overstretching transition of single DNA molecules. *Biophys. J.* 82:3160–3169.
25. Williams, L. D. 2000. Electrostatic mechanisms of DNA deformation. *Annu. Rev. Biophys. Biomol. Struct.* 29:497–521.
26. Yang, Y., I. Tobias, and W. K. Olson. 1993. Finite-element analysis of DNA supercoiling. *J. Chem. Phys.* 98:1673–1686.
27. Bauer, W. R., R. A. Lund, and J. H. White. 1993. Twist and writhe of a DNA loop containing intrinsic bends. *Proc. Natl. Acad. Sci. USA.* 90:833–837.
28. Gromiha, M. M., M. G. Munteanu, A. Gabrielian, and S. Pongor. 1996. Anisotropic elastic bending models of DNA. *J. Biol. Phys.* 22:227–243.
29. Munteanu, M. G., K. Vlahovicek, S. Parthasarathy, I. Simon, and S. Pongor. 1998. Rod models of DNA: sequence-dependent anisotropic elastic modeling of local bending phenomena. *Trends Biochem. Sci.* 23:341–347.
30. Villa, E., A. Balaeff, and K. Schulten. 2005. Structural dynamics of the *lac* repressor-DNA complex revealed by a multiscale simulation. *Proc. Natl. Acad. Sci. USA.* 102:6783–6788.
31. Odijk, T. 1977. Polyelectrolytes near rod limit. *J. Poly. Sci. B Poly. Phys.* 15:477–483.
32. Skolnick, J., and M. Fixman. 1977. Electrostatic persistence length of a wormlike polyelectrolyte. *Macromolecules.* 10:944–948.
33. Manning, G. S. 2006. The persistence length of DNA is reached from the persistence length of its null isomer through an internal electrostatic stretching force. *Biophys. J.* 91:3607–3616.
34. Hagerman, P. J. 1983. Electrostatic contribution to the stiffness of DNA molecules of finite length. *Biopolymers.* 22:811–814.
35. Fenley, M. O., G. S. Manning, and W. K. Olson. 1992. Electrostatic persistence length of a smoothly bending polyion computed by numerical counterion condensation theory. *J. Phys. Chem.* 96:3963–3969.
36. Sanner, M. F., A. J. Olson, and J. C. Spehner. 1996. Reduced surface: an efficient way to compute molecular surfaces. *Biopolymers.* 38:305–320.
37. Heckbert, P. S., and M. Garland. 1999. Optimal triangulation and quadric-based surface simplification. *Comp. Geom. Theor. Appl.* 14:49–65.
38. Mills, P., C. F. Anderson, and M. T. Record. 1985. Monte Carlo studies of counterion DNA interactions—comparison of radial distribution of counterions with predictions of other polyelectrolyte theories. *J. Phys. Chem.* 89:3984–3994.
39. Manning, G. S. 1978. Molecular theory of polyelectrolyte solutions with applications to electrostatic properties of polynucleotides. *Q. Rev. Biophys.* 11:179–246.
40. Shew, C. Y., and A. Yethiraj. 1998. Ion binding in tobacco mosaic virus solutions. *J. Chem. Phys.* 109:5162–5163.
41. Hansen, J. P., and I. R. McDonald. 2007. Theory of Simple Liquids. Academic Press, New York.
42. Patra, C. N., and A. Yethiraj. 1999. Density functional theory for the distribution of small ions around polyions. *J. Phys. Chem. B.* 103:6080–6087.
43. Baker, N. A., D. Sept, S. Joseph, M. J. Holst, and J. A. McCammon. 2001. Electrostatics of nanosystems: application to microtubules and the ribosome. *Proc. Natl. Acad. Sci. USA.* 98:10037–10041.
44. Lu, B. Z., X. L. Cheng, J. F. Huang, and J. A. McCammon. 2006. Order *N* algorithm for computation of electrostatic interactions in biomolecular systems. *Proc. Natl. Acad. Sci. USA.* 103:19314–19319.
45. Banavali, N. K., and B. Roux. 2002. Atomic radii for continuum electrostatics calculations on nucleic acids. *J. Phys. Chem. B.* 106:11026–11035.
46. Im, W., D. Beglov, and B. Roux. 1998. Continuum solvation model: computation of electrostatic forces from numerical solutions to the Poisson-Boltzmann equation. *Comput. Phys. Commun.* 111:59–75.
47. Bomble, Y. J., and D. A. Case. 2008. Multiscale modeling of nucleic acids: insights into DNA flexibility. *Biopolymers.* 89:722–731.
48. Bashford, D., and D. A. Case. 2000. Generalized Born models of macromolecular solvation effects. *Annu. Rev. Phys. Chem.* 51:129–152.
49. Srinivasan, J., M. W. Trevathan, P. Beroza, and D. A. Case. 1999. Application of a pairwise Generalized Born model to proteins and nucleic acids: inclusion of salt effects. *Theor. Chem. Acc.* 101:426–434.
50. Balaeff, A., C. R. Koudella, L. Mahadevan, and K. Schulten. 2004. Modeling DNA loops using continuum and statistical mechanics. *Phil. Trans. Royal Soc. London Series A Math. Phys. Eng. Sci.* 362:1355–1371.
51. Garcia, H. G., P. Grayson, L. Han, M. Inamdar, J. Kondev, et al. 2007. Biological consequences of tightly bent DNA: the other life of a macromolecular celebrity. *Biopolymers.* 85:115–130.
52. Elcock, A. H., and J. A. McCammon. 1996. The low dielectric interior of proteins is sufficient to cause major structural changes in DNA on association. *J. Am. Chem. Soc.* 118:3787–3788.
53. Sun, J., Q. Zhang, and T. Schlick. 2005. Electrostatic mechanism of nucleosomal array folding revealed by computer simulation. *Proc. Natl. Acad. Sci. USA.* 102:8180–8185.
54. Boal, D. 2002. Mechanics of the Cell. Cambridge University Press, Cambridge, UK.
55. Howard, J. 2001. Mechanics of Motor Proteins and the Cytoskeleton. Sinauer Associates, Sunderland, MA.
56. Anishkin, A., C. S. Chiang, and S. Sukharev. 2005. Gain of function mutations reveal expanded intermediate states and a sequential action of two gates in MscL. *J. Gen. Physiol.* 125:155–170.
57. Balaeff, A., L. Mahadevan, and K. Schulten. 2006. Modeling DNA loops using the theory of elasticity. *Phys. Rev. E Stat. Nonlin. Soft Matter Phys.* 73:031919.
58. Zhang, Q., D. A. Beard, and T. Schlick. 2003. Constructing irregular surfaces to enclose macromolecular complexes for mesoscale modeling using the discrete surface charge optimization (DiSCO) algorithm. *J. Comput. Chem.* 24:2063–2074.
59. Brooks, B. R., R. E. Bruccoleri, B. D. Olafson, D. J. States, S. Swaminathan, et al. 1983. CHARMM—a program for macromolecular energy, minimization, and dynamics calculations. *J. Comput. Chem.* 4:187–217.
60. Frenkel, D., and B. Smit. 2002. Understanding Molecular Simulation: From Algorithms to Applications. Academic Press, San Diego, London.